JOURNAL OF SPACECRAFT AND ROCKETS
Vol. 35, No. 1, January–February 1998

Heat Flux on Partially Catalytic Surfaces in Hypersonic Flows

M. Serpico*
Centro Italiano Ricerche Aerospaziali, Capua 81043, Italy
and
R. Monti† and R. Savino‡
University of Naples "Federico II," Naples 80125, Italy

The combined effects of the chemical nonequilibrium and the surface catalysis on the stagnation-point heat flux of a blunt body are investigated by Navier–Stokes calculations on a spherical model under Scirocco Plasma Wind Tunnel conditions. The freestream properties in the test section are found by means of a preliminary nonequilibrium, full Navier–Stokes computation of the nozzle flow expansion. All available numerical heat flux results are correlated as a function of a dimensionless parameter, including the simultaneous effects of the finite-gas and the surface-phase reactions. The proposed parameter, which takes into account simultaneously the nonequilibrium effects in the bulk and surface phases, correlates well with the numerical results over a blunt-body stagnation region. The final correlation formula for the stagnation heat flux can be used to correlate experimental results on different materials with known catalytic coefficients or, conversely, to determine the surface catalytic efficiency of different thermal protection materials.

Nomenclature

a	= speed of sound, m/s
c_p	= specific heat per unit mass at constant pressure, J/kg · K
D	= diffusion coefficient, m²/s
D_a	= homogeneous Damköhler number; Eq. (28)
D_{as}	= heterogeneous Damköhler number; Eq. (31)
E	= total energy, J
$\dot{E}_v$	= vibrational energy source term, J/s
e	= specific total energy per unit volume, J/m³
h	= enthalpy per unit mass, J/kg
h_i^{for}	= heat envolved in the formation of component i, J/kg
k	= Boltzmann constant (1.38022×10^{-23}), J/K
$k_{b,r}$	= backward reaction-rate coefficient for reaction r
$k_{e,r}$	= equilibrium constant for reaction r
$k_{f,r}$	= forward reaction-rate coefficient for reaction r
k_w	= catalytic reaction-rate constant, m/s
M	= molecular weight, kg/kg · mole
n	= normal to the wall coordinate
p	= pressure, Pa
q	= stagnation-point heat flux, W/m²
qm	= mole fraction
Re	= Reynolds number
R_i	= gas constant of component i
r_b	= body radius
Sc	= Schmidt number
T	= absolute temperature, K
u	= x component of velocity, m/s
v	= y component of velocity, m/s
x	= x-axis component
Y	= mass fraction
y	= y-axis component
γ	= recombination coefficient
λ	= thermal conductivity, J/m · s
ρ	= density, kg/m³
τ	= heat flux correlation parameter
$\dot{\omega}$	= catalytic recombination rate, kg/m² · s

Subscripts

a	= atomic species
c	= conductive term
d	= diffusive term
eq	= equilibrium
f	= frozen
fcw	= fully catalytic wall
i	= ith component of mixture
N	= atomic nitrogen
ncw	= noncatalytic wall
ns	= number of chemical species
nvs	= number of vibrational species
O	= atomic oxygen
p	= partial derivative with respect to pressure
t	= partial derivative with respect to time
v	= vibrational term
w	= wall
x, y, z	= Cartesian components
ρ	= partial derivate with respect to density
0	= stagnation conditions
02	= stagnation-point conditions
∞	= freestream value

Superscripts

p	= reaction order for catalytic reaction
$+$	= nondimensional quantities

Introduction

DURING the hypersonic re-entry phase of a space vehicle, the total enthalpy of the freestream is large enough to cause molecular dissociation in the shock layer. The atoms so generated can recombine through the boundary layer, depending on the surface temperature and on the chemical flow conditions (equilibrium, nonequilibrium, frozen). Usually, the segment of the re-entry flight corridor corresponding to the maximum aerodynamic heating is characterized by nonequilibrium conditions in the shock layer. In these conditions the properties of the body surface, as well as the level of the dissociation and how far the gas mixture is from equilibrium conditions, can play an important role in the chemical recombination process. In fact, the atom species can recombine at the wall, providing an additional contribution to the heat transfer, due to species diffusion. This contribution, for a re-entry vehicle, is typically of the same order of magnitude as the Fourier contribution. Because of the complex nonequilibrium phenomena involving the

Received Feb. 21, 1997; revision received July 24, 1997; accepted for publication Aug. 3, 1997.

*Aerospace Engineer, Aerothermodynamics Section, Via Maiorise.
†Full Professor of Aerodynamics, Department of Science and Space Engineering, 80 Piazzale Tecchio. Member AIAA.
‡Aerospace Engineer, Department of Science and Space Engineering, 80 Piazzale Tecchio.

Table 1 Scirocco nozzle exit values

Case	Mach	P, Pa	T, K	Y_O	Y_N	Y_{NO}	Y_{O_2}
A	9.78	2.73	182	0.0404	0.0	0.0432	0.170
B	10.67	2.43	206	0.212	0.0	0.0190	0.011
C	11.80	2.23	217	0.233	0.186	0.0	0.0
D	13.2	1.92	175	0.233	0.424	0.0	0.0
E	7.95	47.62	292	0.0255	0.0	0.050	0.181
F	8.20	44.58	400	0.166	0.0	0.031	0.050
G	8.66	42.55	510	0.231	0.125	0.0	0.0
H	9.49	32.42	450	0.233	0.335	0.0	0.0
I	7.47	182.38	571	0.109	0.0	0.0422	0.102

chemical species both in the shock layer and on the model surface, a rigorous analysis of the problem is required. The theory of the stagnation-point heat flux in a dissociating gas has been introduced by Fay and Riddel,[1] for equilibrium or frozen boundary layers, in the extreme situations of a fully catalytic or a noncatalytic surface. After this pioneering work, Goulard[2] addressed the problem of the partial catalytic activity of the surfaces, neglecting nonequilibrium chemical effects in the boundary layer (which was supposed frozen). All of the results of these studies were obtained with boundary-layer calculations, using simplified models for the transport properties. Many other researchers have investigated, with advanced computational fluid dynamics (CFD) tools, the effects produced on the stagnation-point heat transfer by the nonequilibrium freestream conditions or by the partially catalytic surfaces separately[3,4]; in this paper, a systematic analysis concerning the combined effects of chemical nonequilibrium flows and partially catalytic surfaces is performed. A full Navier–Stokes code, including the effects of nonequilibrium chemical reactions and vibrational relaxation, is used to obtain a general relationship of the stagnation-point heat flux in the presence of a recombination process with finite surface catalytic activity. A new correlation formula is proposed for an engineering prediction of the heat flux in nonequilibrium hypersonic flow.

Scirocco Plasma Wind Tunnel

The Scirocco project is a European program devoted to the development of a 70-MW, arc-heated hypersonic facility, referred to as the plasma wind tunnel (PWT). This facility is being constructed at Centro Italiano Ricerche Aerospaziali in Capua, Italy, to be used for experimental measurements on thermal protection system materials of entry space vehicles. The main characteristics of this facility are the very high stagnation conditions, in terms of total enthalpy and total pressure, and the possibility of testing large-scale models, up to about 2 m.

The gas in the Scirocco is heated by a 5.5-m-long arc heater, accelerates through convergent–divergent nozzles, and enters the test chamber at high Mach numbers; downstream from the test chamber, there is a diffuser and a heat exchanger. The complete aerothermodynamic process was studied in the design phase. On the basis of the performances of this facility, a numerical analysis of the heat flux on a spherical partially catalytic body located in the test section has been developed. The test envelope is shown in Fig. 1, where the performances of the Scirocco PWT are illustrated. The freestream conditions for the spherical model are shown in Table 1. These conditions have been determined by solving with the nonequilibrium Navier–Stokes code the hypersonic flow expansion in the conical nozzle of Scirocco.[5]

Mathematical Model

Assuming that the air is a mixture of five different species (O, N, NO, O_2, and N_2) in chemical and vibrational nonequilibrium, the laminar Navier–Stokes equations for axisymmetric flows are written in the integral form as

$$\frac{\partial}{\partial t}\int_V \boldsymbol{W}\,\mathrm{d}V + \int_S \boldsymbol{F}\cdot\boldsymbol{n}\,\mathrm{d}S = \int_V \boldsymbol{G}\,\mathrm{d}V - \frac{1}{y}\int_V (\boldsymbol{H}+\boldsymbol{H}_v)\,\mathrm{d}V \quad (1)$$

where

$$\boldsymbol{W} = [\rho_i\ ,\ \rho\ ,\ \rho u,\ \rho v,\ e,\ \rho E_{vj}]^T \quad (1a)$$

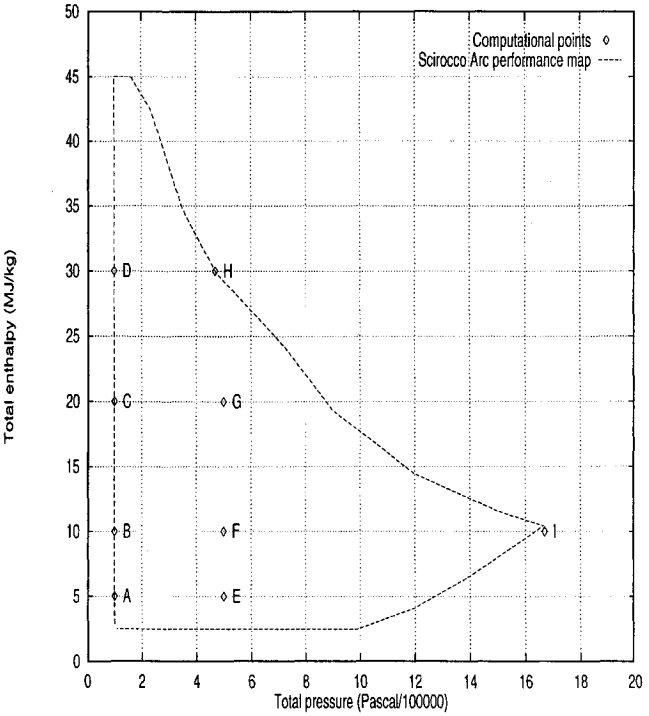

Fig. 1 Analyzed points within the Scirocco arc performance map.

$$\boldsymbol{F} = (\boldsymbol{F}_{x,\mathrm{inv}} - \boldsymbol{F}_{x,\mathrm{vis}},\ \boldsymbol{F}_{y,\mathrm{inv}} - \boldsymbol{F}_{y,\mathrm{vis}}) \quad (1b)$$

$$\boldsymbol{F}_{x,\mathrm{inv}} = \left[\rho_i u,\ \rho u,\ \rho u^2 + p,\ \rho uv,\ (p+e)u,\ \rho E_{vj}u\right]^T \quad (1c)$$

$$\boldsymbol{F}_{y,\mathrm{inv}} = \left[\rho_i v,\ \rho v,\ \rho uv,\ \rho v^2 + p,\ (p+e)v,\ \rho E_{vj}v\right]^T \quad (1d)$$

$$\boldsymbol{F}_{x,\mathrm{vis}} = [j_{i,x},\ 0,\ \tau_{xx},\ \tau_{xy},\ u\tau_{xx} + v\tau_{xy} + q_x,\ q_{v,x}]^T \quad (1e)$$

$$\boldsymbol{F}_{y,\mathrm{vis}} = [j_{i,y},\ 0,\ \tau_{xy},\ \tau_{yy},\ u\tau_{xy} + v\tau_{yy} + q_y,\ q_{v,y}]^T \quad (1f)$$

$$\boldsymbol{G} = [\Omega_i,\ 0,\ 0,\ 0,\ 0,\ \rho\dot{E}_{vj}]^T \quad (1g)$$

$$\boldsymbol{H} = \left[\rho_i v,\ \rho v,\ \rho vu,\ \rho v^2,\ v(p+e),\ \rho vE_{vj}\right]^T \quad (1h)$$

$$\boldsymbol{H}_v = [j_{i,y},\ 0,\ \bar{\tau}_{xy},\ \bar{\tau}_{xx},\ \bar{\tau} + q_y,\ q_{v,y}]^T \quad (1i)$$

where the subscript $i = 1$, ns $-$ 1, and $j = 3, 3 +$ nvs $-$ 1. In the present work, ns $= 5$ and nvs $= 3$.

Equation (1) includes the mass balance of the species O, N, NO, and O_2. The quantity Ω_i/ρ represents the rate of production of the species, and the partial density ρ_i can be expressed in terms of the mixture density ρ and the mass concentration Y_i as

$$\rho_i = \rho Y_i \quad (2)$$

The concentration Y_{N_2} of molecular nitrogen follows from the conservation of the atomic species.

The quantities $\dot{E}_{v_j}$ are the rates of production of the vibrational energies of the molecular species O, O_2, and N_2. The thermodynamic enthalpy of the mixture is defined by

$$h = \sum_{i=1}^{ns} Y_i c_{pi} T + \sum_{i=1}^{ns} Y_i h_i^{for} + \sum_{j=3}^{3+nvs-1} Y_j E_{vj} \tag{3}$$

The species diffusion fluxes along the x direction are based on Fick's law of diffusion,

$$j_{i,x} = D_i \rho \frac{\partial Y_i}{\partial x} \tag{4}$$

This expression is an approximation because Fick's law holds rigorously only for a binary mixture; however, it can be applied reasonably well also in this case because the differences between the molecular weights of the species considered are not large.[6]

The conductive, chemical, and vibrational parts of the total heat flux along the x direction are defined by

$$q_{c,x} = \lambda \frac{\partial T}{\partial x} \tag{5}$$

$$q_{d,x} = \sum_{i=1}^{ns} \rho D_i h_i \frac{\partial Y_i}{\partial x} \tag{6}$$

$$q_{v,x} = \sum_{j=3}^{3+nvs-1} \rho D_j E_{vj} \frac{\partial Y_j}{\partial x} \tag{7}$$

and likewise in the y direction.

The axisymmetric viscous contributions (considered as source terms) read

$$\bar{\tau}_{xy} = \frac{2}{3} y \frac{\partial(\mu v/y)}{\partial x} - \tau_{xy} \tag{8}$$

$$\bar{\tau}_{xx} = \frac{2}{3} y \frac{\partial(\mu v/y)}{\partial y} - \tau_{yy} + \frac{2}{3}\frac{\mu v}{y} + \tau_{\theta\theta} \tag{9}$$

$$\bar{\tau} = u\tau_{xy} + v\tau_{yy} - \tfrac{2}{3}\mu v^2 y \tag{10}$$

The transport properties were calculated using the Chapman–Cowling[7] theoretical model of the intermolecular potential; the collisions integrals to be used in these formulations were obtained from the Yun–Mason[8] theory.

Thermokinetic Model

The chemical model used is the well-known Park model,[9] characterized by 17 reactions involving the five species (O, N, NO, O_2, and N_2). The ionization processes are neglected in the present study; in general, the flow behavior in an arc-heated PWT may be very complicated because of the presence in the flow of ions and electrons formed at the arcjet. If the arc-heated flow is suddenly expanded in the nozzle, only partial equilibrium may be reached, so that a certain level of ionization may be present in the freestream. In the Scirocco PWT, before the flow expands in the nozzle, it crosses a plenum chamber, achieving equilibrium. For the conditions investigated in the present work, with a maximum total enthalpy level of 30 MJ/kg, the electron and ion concentrations can be neglected because the corresponding equilibrium total temperature is about 7000 K. (Ionization processes take place at air temperature greater than 9000 K; see Ref. 10.)

The reaction rate constants are given by

$$K_{f,r} = c_r T_{ai}^{n_f} \exp(-D_r/kT_{ai}) \tag{11}$$

$$K_{b,r} = K_{f,r}/K_{e,r}, \qquad r = 1, \ldots, 17 \tag{12}$$

$$K_{e,r} = \exp\left[\sum_{i=1}^{ns} A_{ir} Z^{(i-1)}\right] \tag{13}$$

in which $Z = 10{,}000/T$ and the constants A_{ir}, c_r, D_r, and n_f are given[9]; in Eq. (10), the temperature T_{ai} is equal to $(TT_{vi})^{1/2}$. The expressions used for the frozen specific heats c_{pi} are

$$c_{pi} = (n/2)R_i, \qquad i = 1, \ldots, \text{ns} \tag{14}$$

where n is 5 for monoatomic and 7 for diatomic species.

Translational–vibrational interspecies relaxation is modeled according to the Millikan–White theory.[11]

Boundary Conditions

The boundary conditions are imposed along the edges of the computational domain. The freestream conditions are enforced at the far-field boundary, and zero-order extrapolation conditions are set at the supersonic outflow. Along the stagnation line, symmetry conditions are imposed. On the solid wall, the no-slip condition for velocity is considered and the temperature is prescribed (T_w). Furthermore, the conditions for the chemical composition on the body surface must be specified. When nonequilibrium conditions prevail in the boundary layer near the wall, the atoms produced by the dissociation reactions (behind the shock) strike the surface. The general boundary conditions for a catalytic wall are obtained imposing steady-state mass atomic conservation at the wall, i.e., the amount of species formed at the surface due to the catalytic recombination rate $\dot{\omega}$ must be balanced by the rate of diffusion to the surface:

$$(\dot{\omega}_a)_w = -(\rho_a v_a)_w \tag{15}$$

The diffusive flux $\rho_a v_a$ is expressed with the usual Fick's law; that projected along the direction normal to the wall reads

$$\rho_a v_a = -\rho D_{ma}\left(\frac{\partial Y_a}{\partial n}\right) \tag{16}$$

The source term in Eq. (15) is given by Goulard's relation[2]

$$\dot{\omega}_a = K_{wa}(\rho_w Y_{iw})^p \tag{17}$$

The catalytic reaction-rate constant K_{wa} is related to the recombination probability γ by means of the Hertz–Knudsen relation[12]

$$K_{wa} = \gamma\sqrt{kT_w/2\pi m_a} \tag{18}$$

Assuming a noncatalytic wall boundary condition for nitrogen oxide (NO) and a first-order reaction for the other species, the atomic species mass fractions at the wall are computed by Eqs. (15–17). Imposing the condition that oxygen atoms are conserved at the wall, the molecular oxygen is calculated as

$$\left(\frac{\partial Y_{O_2}}{\partial n}\right)_{\text{wall}} = -\left(\frac{\partial Y_O}{\partial n}\right)_{\text{wall}} \tag{19}$$

The molecular nitrogen at the wall is obtained by the continuity equation.

Numerical Formulation

The numerical solution of Eq. (1) has been obtained using a finite volume technique with a central formulation over structured meshes. The inviscid fluxes at cell interfaces are calculated by a flux difference splitting (FDS) Riemann solver with a second-order, essentially nonoscillatory-like approximation.[13] The viscous fluxes are discretized by central differencing: In particular, the gradients of the variables at the cell interfaces are computed using the Gauss theorem. The integration in time is performed by an Euler forward single-stage algorithm, with an implicit evaluation of the source terms.

The basic steps of the FDS formulation are the definition and solution of appropriate Riemann problems. These aspects are highlighted hereinafter; see Ref. 13 for further details.

The solution is considered as piecewise constant over each cell mesh at fixed time, and the evolution of the flow to the next time step results from the wave interactions originating at the boundaries between adjacent cells. The interface between two cells, e.g., N, M and $N+1, M$, with the coordinate normal to the interface denoted by ξ, is a discontinuity surface located at $\xi_{N+(1/2),M}$ (Fig. 2) between the two different fluid states at the left and the right sides. The velocity vector is decomposed into the normal u and tangential v components

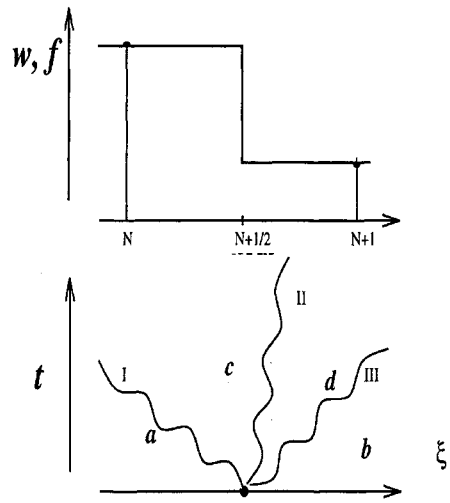

Fig. 2 Interpretation of initial data and collapse of the discontinuity.

to the surface, and the numerical fluxes at the cell boundary are obtained from the solution of the Riemann problem in the direction normal to the interface:

$$qm_{it} + uqm_{i\xi} = 0, \qquad i = 1, \text{ns} \tag{20}$$

$$p_t + up_\xi + \rho a_f^2 u_\xi = 0 \tag{21}$$

$$u_t + uu_\xi + (p_\xi/\rho) = 0 \tag{22}$$

$$v_t + uv_\xi = 0 \tag{23}$$

$$h_t - (p_t/\rho) + u[h_\xi - (p_\xi/\rho)] = 0 \tag{24}$$

$$E_{vjt} + uE_{vj\xi} = 0, \qquad j = 3, 3 + \text{nvs} - 1 \tag{25}$$

Equations (20–25) are obtained from the general equation (1), neglecting dissipative fluxes and source terms and looking for the propagation of disturbances in the ξ direction. The chemical reactions and vibrational relaxation process are considered frozen after the collapse of the discontinuity. The frozen speed of sound, which appears in the continuity equation, is defined by

$$a_f^2 = \frac{h_\rho}{1/\rho - h_p} \tag{26}$$

With reference to Fig. 2, the values at the centers of the two neighboring cells correspond to those prescribed in the regions a and b. Because of the assumption of frozen chemistry and vibrations after the collapse of the discontinuity, the initial level of energy in the regions a and b, given by the initial data and generally different from each other, remain unchanged through the acoustic waves (I and III) in the regions c and d, respectively. On the contact surface (wave II), we impose the usual continuity of the pressure and velocity. In the case of five species and three vibrating molecules, the number of equations is equal to 10, ns = 5, and nvs = 3; the inviscid-flux vector at the interface is defined on the basis of the flow properties that pertain to region c. For more details, see Ref. 13.

Model Validation

The code used in the present work has been extensively tested and validated by computing different flowfields such as blunt body, control surface geometries, and base flow; a detailed description of the results can be found in Refs. 14–16.

Herein, a comparison with other numerical results concerning the hypersonic flow around the scale model of the space probe Electre is reported. The geometry consists of a conical surface with total length of 40 cm, semiangle of 4.6 deg, and hemispherical nose with radius of 3.5 cm. This geometry recently has been considered as a reference geometry to study nonequilibrium hypersonic flows on blunt-body configurations. Numerical and experimental fully catalytic results on the Electre model, in F4 and HEG wind tunnel conditions, have been compared.[14]

Table 2 HEG nozzle exit conditions

U_∞, m/s	5919.0
ρ_∞, kg/m^3	1.64×10^{-3}
L, m	0.4
T_∞, K	790.0
Tv_∞, K	790.0
Mach	9.70
Y_O	0.179
Y_N	1.0×10^{-6}
Y_{NO}	3.30×10^{-2}
Y_{O_2}	3.60×10^{-2}

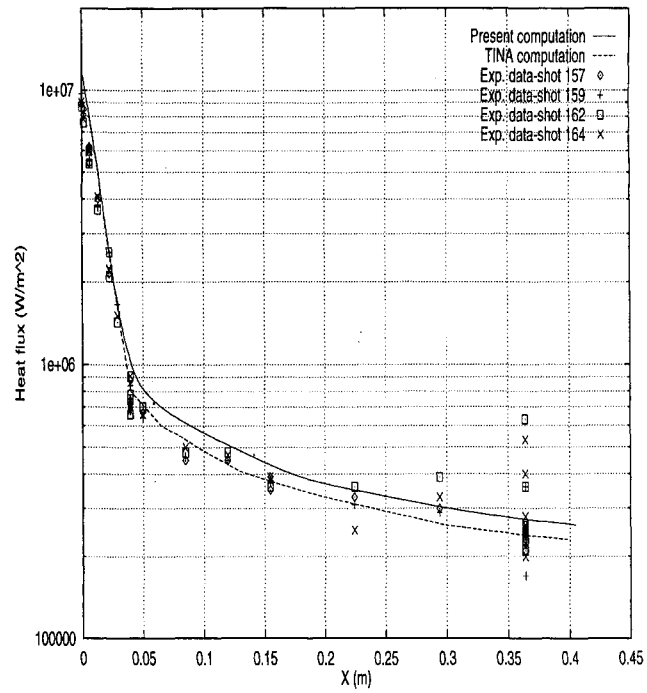

Fig. 3 Computed heat fluxes for the Electre model, in HEG wind tunnel, with a fully catalytic wall.

In Fig. 3, the numerical and experimental heat fluxes are compared. The numerical results obtained with the TINA code,[17] a three-dimensional, time-marching Navier–Stokes solver including chemical nonequilibrium, also are shown. The mesh is the same for both numerical computations, with $\Delta n^+ = 1.11 \times 10^{-3}$ at the wall in the stagnation region. The freestream conditions, corresponding to the free piston shock tunnel HEG in Göttingen, Germany, are reported in Table 2. The results show a satisfactory agreement between the two numerical computations even if some differences are present along the conical part of the body. In comparison with the experimental results, the CFD results give a numerical overprediction of the heat flux in the stagnation region but compare well in the first part of the conical part of the body. At the end of the Electre probe, a large spread of experimental data is present, indicating some experimental measurement difficulties in this region.

Flowfield Around the Specimen

A parametrical analysis has been developed to investigate the velocity, temperature, and concentration distributions in the viscous shock layer surrounding different spherical models at the freestream conditions corresponding to the different points within the Scirocco arc performance map (Fig. 1). For each point of the map, i.e., for prescribed conditions in the test chamber, two different spheres with radius $r_b = 0.3$ and 0.03 m are considered, assuming different values of the catalytic efficiency. A preliminary analysis shows that grid independency on the flow solution is obtained with 2400 grid points (60×40). To account for the different Reynolds number, different values of the stretching parameter are used for the two different

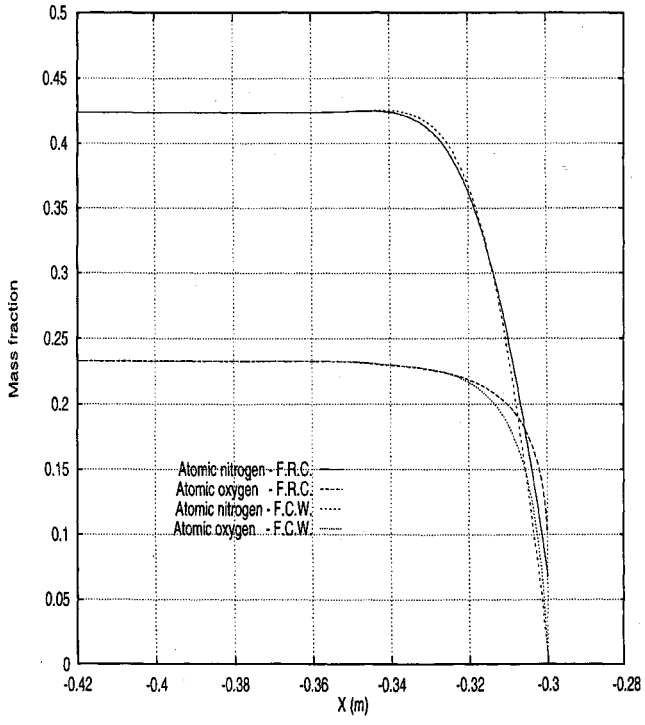

Fig. 4 Computed distribution of atomic oxygen along the stagnation streamline for a surface with partial catalytic activity ($\gamma_O = \gamma_N = 0.1$), total enthalpy ($H_0 = 30$ MJ/kg), and two different values of the stagnation pressure ($p_0 = 470{,}000$ and 100,000 Pa).

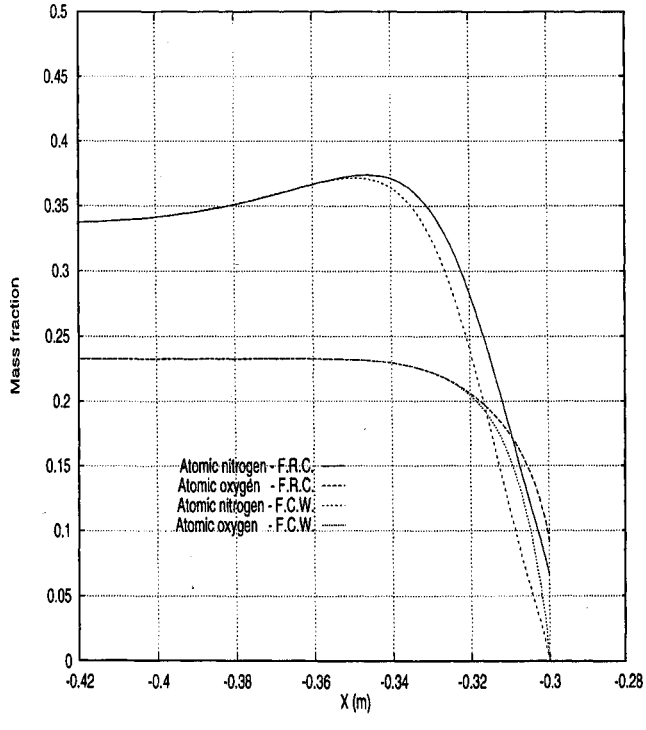

Fig. 5 Computed distribution of atomic nitrogen along the stagnation streamline for the same conditions as in Fig. 4.

geometries ($r_b = 0.3$ and 0.03 m) with Δn^+ at the wall in the stagnation region of 2.47×10^{-3} and 2.0×10^{-2}, respectively. The origin of the x axis is located in correspondence to the stagnation point of the body surface. Figures 4 and 5 show the computed distributions of atomic oxygen and nitrogen along the stagnation streamline for a fully catalytic wall and a surface with a finite rate chemistry having $\gamma_O = \gamma_N = 0.1$; the computations are performed in correspondence to the same total enthalpy ($H_0 = 30$ MJ/kg) with two different values of the stagnation pressure ($p_0 = 470{,}000$ and 100,000 Pa). The results indicate that the influence of the wall catalysis is directly related to the chemical nonequilibrium conditions in the shock layer. In particular, when the pressure increases, the gas approaches the equilibrium conditions, so that the dissociated species tend to recombine spontaneously in the cold boundary layer near the wall and the driving effect of the catalytic wall becomes negligible. Similar behavior occurs if the body radius is large, e.g., for $r_b = 0.3$ m. Conversely, if the pressure or the body radius is small, the chemical conditions in the shock layer are close to the frozen equilibrium, so that the influence of the catalytic wall effect on the stagnation-point heat flux becomes large.

Stagnation-Point Heat-Flux Numerical Correlation

As discussed in the preceding section, the influence of the catalytic properties of the wall on the aerodynamic heat flux depends on the chemical state of the gas in the shock layer. This aspect is not taken into account during experimental measurements in hypersonic facilities based on the use of classical simplified engineering formulas, e.g., Ref. 1. To analyze the simultaneous effects of the bulk kinetic rates and of the surface catalysis and to provide an extended engineering correlation formula based on the CFD results, the numerically computed stagnation-point heat fluxes are correlated as a function of the two relevant dimensionless parameters characteristic of the chemical reaction effects in the shock layer and on the body surface. Attention has been focused on the chemical reaction involving molecular and atomic oxygen because, for the conditions investigated, the most relevant chemical contribution to the heat flux comes from the oxygen recombination process at the wall. The inviscid equation for the atomic oxygen reads

$$u\frac{\partial Y_O}{\partial x} + v\frac{\partial Y_O}{\partial y} = \frac{\dot{\omega}_O}{\rho} \tag{27}$$

Using the classical law of the mass equation for the recombination reaction rate and dividing by the characteristic convective time, Eq. (27) can be posed in the nondimensional form

$$u^+\frac{\partial Y_O}{\partial x^+} + v^+\frac{\partial Y_O}{\partial y^+} = D_a\rho^+ \tag{28}$$

where the homogeneous Damköhler number $Da = K_1[(\rho_{ref}L_{ref})/V_{ref}]$ is the ratio between a characteristic permanence time $t_p = L_{ref}/V_{ref}$ divided by the gas reaction time $t_b = 1/(K_1\rho_{ref})$. When $Da \to \infty$, the gas in the shock layer is in chemical equilibrium, whereas in the other extreme, $Da = 0$, the flow is frozen. K_1 has the following expression:

$$K_1 = (2/M_O)(1 + Y_O)K_b\left[(1 - Y_O)/(\rho^+K_e) - Y_O^2\right] \tag{29}$$

Assuming that the catalytic recombination of atoms at the body surface is governed by a first-order rate law, the boundary condition at the catalytic wall, in nondimensional form, reads

$$\left(D_i^+\frac{\partial Y_i}{\partial n^+}\right)_w = Y_{wi}D_{as} \tag{30}$$

where

$$D_{as} = \left(\frac{K_{wi}L_{ref}}{D_{ref}}\right) \tag{31}$$

The dimensionless parameter D_{as} (heterogeneous Damköhler number) is the ratio between the characteristic local diffusion time $t_d = L_{ref}^2/D_{ref}$ to the surface recombination time $t_s = L_{ref}/K_{wi}$ expressed in terms of the atom recombination velocity K_w on the surface. The parameter K_w is a (known) function of the wall temperature and depends on the surface catalytic efficiency of the material. When $D_{as} \to \infty$, the surface is completely catalytic ($Y_{O_w} = 0$), whereas in the case $D_{as} = 0$, the surface is noncatalytic and the diffusion flux of atoms at the wall is zero. The numerical results obtained for the two different geometries investigated ($r_b = 0.03$ and 0.3 m) for the eight test-chamber conditions reported in Table 1, in correspondence to four different values of the catalytic efficiency (∞, 0.1, 0.01, and 0), are summarized in Fig. 6. The nondimensional parameter $\phi = (q - q_{ncw})/(q_{fcw} - q_{ncw})$, taking into account the heat flux due to the surface catalytic activity (divided by the maximum heat flux difference, corresponding to the extreme situations of fully

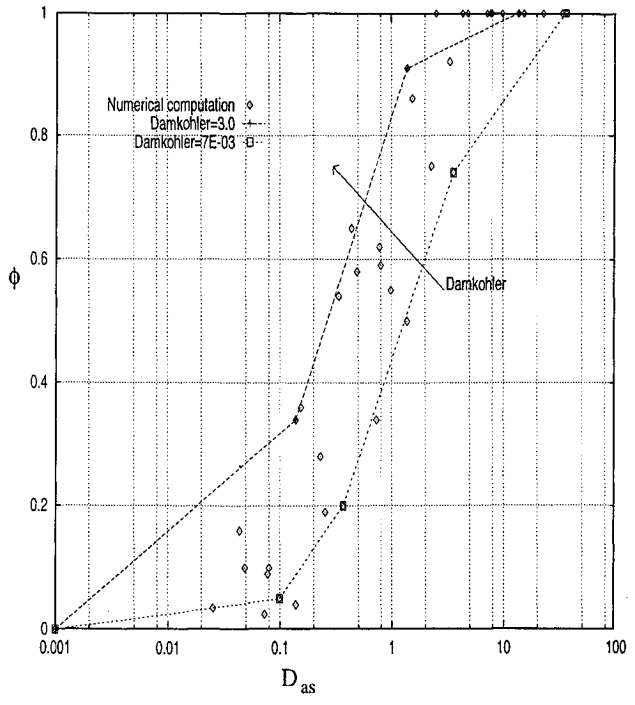

Fig. 6 Nondimensional stagnation-point heat flux as a function of the heterogeneous Damköhler number D_{as} for different values of the homogeneous Damköhler number D_a.

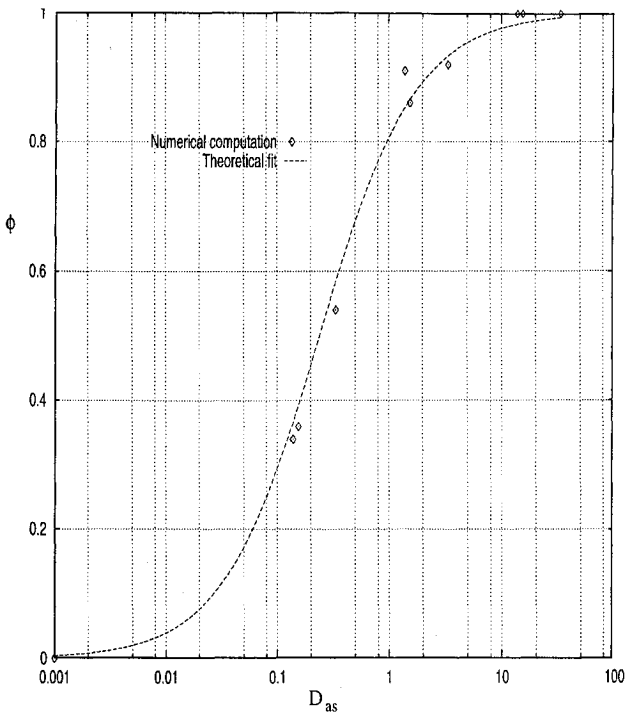

Fig. 7 Interpolation curve obtained for D_a = 3.0.

catalytic and noncatalytic wall), is reported as a function of D_{as} for different values of the homogeneous Damköhler number Da. We see that the stagnation-point heat flux increases with the parameter D_{as} and that, for an assigned D_{as}, it is an increasing function of D_a. On the basis of these results, a first correlation law as a function of D_{as} has been determined for fixed D_a:

$$\phi = \frac{q - q_{\text{ncw}}}{q_{\text{fcw}} - q_{\text{ncw}}} = \frac{D_{as}}{A + BD_{as}} \tag{32}$$

Figure 7 shows the interpolation law obtained for $D_a = 3.0$. For the two coefficients A and B, the following functional dependences were found in the whole range investigated:

$$A = 1.2 - \exp(-0.1/Da), \qquad B = 1 \tag{33}$$

By using these equations, the following expression of ϕ was found:

$$\frac{q - q_{\text{ncw}}}{q_{\text{fcw}} - q_{\text{ncw}}} = \frac{1}{1 + \tau} \tag{34}$$

where τ has the following expression:

$$\tau = \frac{1.2 - \exp(-0.1/Da)}{D_{as}} \tag{35}$$

The numerical correlation of the diffusive heat flux is given in Fig. 8 as a function of the heterogeneous Damköhler number D_{as} and for different values of the homogeneous Damköhler number Da. The parameter τ represents a new correlation parameter for heat fluxes on partially catalytic surfaces in chemical nonequilibrium, as shown in Fig. 9. All of the numerical results correlate well with the proposed law.

Equation (34) gives the heat flux for the general case of chemical nonequilibrium and partially catalytic surface. The fully catalytic and noncatalytic limits are obtained as particular cases for $D_{as} \to \infty (\tau = 0)$ and for $D_{as} \to 0 (\tau \to \infty)$.

Similar results also were found by Inger,[18] i.e., applying integral methods to boundary-layer theory obtained correlations of the stagnation heat flux with homogeneous and heterogeneous Damköhler numbers. The theory was developed under a large number of simplifying approximations regarding the flow chemistry and the transport properties in the shock layer. The nondimensional parameter $(q - q_f)/(q_{\text{eq}} - q_f)$ was expressed in terms of a composite

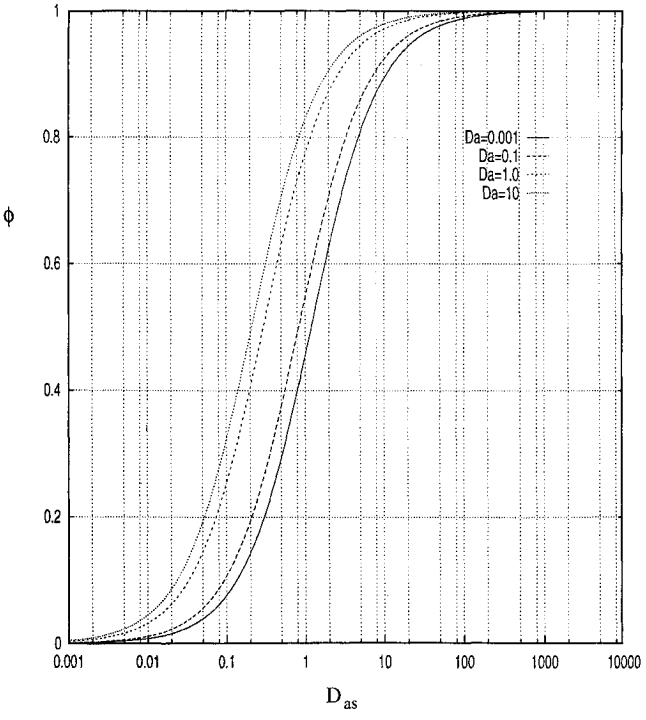

Fig. 8 Correlation parameter ϕ vs D_{as} and D_a.

Damköhler number that, similar to the actual correlation parameter τ, represents the simultaneous effects of the finite-gas-phase and surface reaction rates. According to this formula, the stagnation-point heat flux can be determined as a function of the two Damköhler numbers once the frozen and the equilibrium values are known. In the present work the correlation parameter τ gives a very simple equation for evaluation of the function $(q - q_{\text{ncw}})/(q_{\text{fcw}} - q_{\text{ncw}})$. The effect of the surface catalysis can be evaluated directly because only q is a function of the heterogeneous Damköhler number D_{as}, q_{ncw} and q_{fcw} being functions of the homogeneous Damköhler number only, whereas in the Inger correlation formula, the frozen heat flux was strongly dependent on the catalytic efficiency. Comparing Eq. (34) to the correlation equation obtained by Inger, we see that, although the two approaches are completely different, a very similar dependence

Table 3 CARINA flight re-entry data

Altitude, km	p_{02}, Pa	H_0, MJ/kg
89.5	204.67	27.8
80.7	898.75	26.9
69.9	4083.40	24.1
59.9	1063.91	17.7
48.4	20,265	8.60

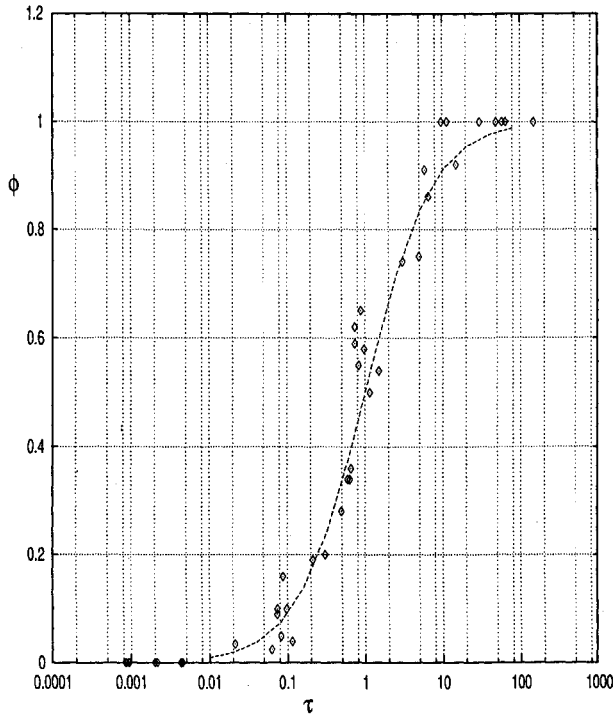

Fig. 9 Nondimensional stagnation-point heat flux as a function of the correlation parameter τ.

of the stagnation-point heat flux upon the heterogeneous Damköhler parameter for the frozen boundary-layer case is found. In fact, according to Eq. (34), for $D_a \to 0, \phi \to D_{as}/(1.2 + D_{as})$, whereas the Inger formula for the frozen boundary layer and unitary Lewis number gives $\phi \to \zeta_w/(1 + \zeta_w)$, where ζ_w is the heterogeneous Damköhler number introduced by Inger.

The stagnation-point heat-flux correlation obtained in the present work (Eq. 34) has been simplified to obtain an engineering formula. In fact, we observe that the homogeneous and heterogeneous Damköhler numbers depend on the following relevant problem data:

$$D_{as} = D_{as}(\gamma, T_w, r_b \times p_{02}, H_0) \tag{36}$$

$$D_a = D_a(r_b \times p_{02}, H_0) \tag{37}$$

According to Eqs. (36) and (37), for a prescribed material with constant temperature, both parameters depend on the total enthalpy H_0 and on the product $r_b \times p_{02}$. The contribution related to the total enthalpy does not change very much in the zone of the reentry corridor with significant aerodynamic heating, as illustrated by Table 3, which reports the typical data for the Italian re-entry capsule CARINA. In this case the total enthalpy H_0 is reduced by a factor of one-third only; conversely, the stagnation-point pressure p_{02} increases by two orders of magnitude. Therefore, during experimental measurements in simulated nonequilibrium flows in hypersonic wind tunnels, the stagnation-point heat flux depends mainly on the product of the stagnation pressure multiplied by the body radius. If the terms on the right-hand side of Eq. (32) are expressed as a function of $r_b \times p_{02}$, the following simple correlation formula is obtained on the basis of the CFD results:

$$\phi = \frac{(r_b \times p_{02})^{\alpha}}{\exp(2 \times \alpha)} - \frac{H_0^2}{30} \tag{38}$$

with

$$\alpha = \frac{1}{(40 \times \gamma^{0.7})} \tag{39}$$

and $r_b \times p_{02}$ (in atm cm).

Conclusions

The nonequilibrium fields around blunt bodies have been computed by a Navier–Stokes code accounting for the effects of nonequilibrium chemical reactions and vibrational relaxation in the bulk phase in the presence of a finite surface catalytic activity. A parametrical analysis has been developed to investigate the velocity, temperature, and concentration distributions in the viscous shock layer surrounding different spherical models at the freestream conditions corresponding to different points within the Scirocco arc performance map. The computed stagnation-point heat fluxes have been correlated as a function of a dimensionless parameter, including the simultaneous effects of the finite-gas- and surface-phase reactions. The scaling parameter, defined in terms of the homogeneous and heterogeneous Damköhler numbers, correlates satisfactorily with the numerical results. The implications of the generalized formula for the experimental measurements of stagnation-point heat flux have been discussed.

References

[1]Fay, J. A., and Riddel, F. R., "Theory of Stagnation Point Heat Transfer in Dissociated Air," *Journal of the Aeronautical Sciences*, Vol. 25, Feb. 1958, pp. 73–85.

[2]Goulard, R. J., "On Catalytic Recombination Rates in Hypersonic Stagnation Heat Transfer," *Jet Propulsion*, Vol. 28, Nov. 1958, pp. 737–745.

[3]Gocken, P., "Effects of Freestream Nonequilibrium on Convective Heat Transfer to a Blunt Body," *Journal of Thermophysics and Heat Transfer*, Vol. 10, No. 2, 1996, pp. 234–241.

[4]Miller, J. H., Tannehill, J. C., Edwards, T. A., and Scott, L. L., "Computation of Hypersonic Flows with Finite Catalytic Wall," AIAA Paper 94-2354, June 1994.

[5]De Filippis, F., Schettino, A., Serpico, M., and Borrelli, S., "Complete Analytical Model to Describe the Test Leg of Scirocco PWT," *Proceedings of the 20th Congress of the International Council of the Aeronautical Sciences*, Vol. 1, AIAA, Reston, VA, 1996, pp. 834–841 (Paper ICAS-96-2.4.5).

[6]Barbato, M., Giordano, D., and Bruno, C., "Comparison Between Finite Rate and Other Catalytic Boundary Conditions for Hypersonic Flows," AIAA Paper 94-2074, June 1994.

[7]Chapman, S., and Cowling, T. G., *The Mathematical Theory of Non-Uniform Gases*, 3rd ed., Cambridge Univ. Press, Cambridge, England, UK, 1970.

[8]Yun, K. S., and Mason, E. A., "Collisional Integrals for the Transport Properties of Dissociating Air at High Temperatures," *Physics of Fluids*, Vol. 5, No. 4, 1962, pp. 380–386.

[9]Park, C., "A Review of Reaction Rates in High Temperature Air," AIAA Paper 89-1740, June 1989.

[10]Bertin, J. J., *Hyperson Aerothermodynamics*, AIAA Education Series, AIAA, Washington, DC, 1994, pp. 56, 57.

[11]Millikan, R. C., and White, D. R., "Systematics of Vibrational Relaxation," *Journal of Chemical Physics*, Vol. 39, No. 12, 1963, pp. 3209–3213.

[12]Scott, C. D., "Effects of Nonequilibrium and Wall Catalysis on Space Shuttle Heat Transfer," *Journal of Spacecraft and Rockets*, Vol. 22, No. 6, 1985, pp. 489–499.

[13]Pandolfi, M., *On the Flux Difference Splitting Formulation*, Vol. 24, Notes on Numerical Fluid Mechanics, Viewig, Braunschweig, Germany, 1989.

[14]Serpico, M., Schettino, A., and Borrelli, S., "MSTP WORKSHOP 1996—Contributions to Electre Model in F4 and HEG Conditions," Workshop on Reentry Aerothermodynamics and Ground to Flight Extrapolation, CIRA-TN-96-047, Noordwijk, The Netherlands, March 1996.

[15]Serpico, M., Schettino, A., Ciucci, A., Falconi, D., and Fabrizi, M., "Vega Launcher Base Flow Prediction at Different Supersonic Mach Numbers," AIAA Paper 97-2302, June 1997.

[16]De Filippis, F., Serpico, M., Marini, M., Ravachol, M., and Tribot, J. P., "Comparison Between Numerical and Experimental Results on Different HERMES Elevon Shapes," *Journal of Spacecraft and Rockets*, Vol. 34, No. 3, 1997, pp. 272–278 (AIAA Paper 96-2472).

[17]Netterfield, N. P., "Validation of a Navier–Stokes Code for Thermochemical Nonequilibrium Flows," AIAA Paper 92-2878, July 1992.

[18]Inger, G. R., "Nonequilibrium Stagnation Point Boundary Layer with Arbitrary Surface Catalycity," *AIAA Journal*, Vol. 1, No. 8, 1963, pp. 1776–1784.

I. E. Vas
Associate Editor